

# Instability and decomposition on the surface of strained alloy films

Zhi-Feng Huang\* and Rashmi C. Desai†  
*Department of Physics, University of Toronto,  
 Toronto, Ontario, Canada M5S 1A7*

A continuum dynamical model is developed to determine the morphological and compositional instabilities on the free surface of heteroepitaxial alloy films in the absence of growth. We use linear stability analysis to study the early nonequilibrium processes of surface evolution, and calculate the stability conditions and diagrams for different cases of material parameters. There are two key considerations in our treatment: the coupling between top free surface of the film and the bulk phase underneath, and the dependence of both Young's and shear elastic moduli on local composition. The combination and interplay of different elastic effects caused by lattice misfit between film and substrate (misfit strain), composition dependence of film lattice parameter (compositional strain) and of film elastic constants lead to complicated and rich stability results, in particular the joint stability or instability for morphological and compositional profiles, the asymmetry between tensile and compressive layers, as well as the possible stabilization and suppression of surface decomposition even below the effective critical temperature. We also compare our results with the observations of some postdeposition annealing experiments.

## I. INTRODUCTION

Instability is one of the most important phenomena in strained heteroepitaxial growth, where a thin film of different material is epitaxially deposited on a substrate and the mismatch of lattice constants between film and substrate leads to strain in the grown film. Besides the formation of misfit dislocations and other defects, the strain can be relieved through the process of morphological instability, during which the growth mode of the film is changed from layer-by-layer to three-dimensional island but the film still remains coherent with its substrate. This dislocation-free morphological instability occurs in a wide range of heteroepitaxial systems, and has been well investigated both theoretically<sup>1,2,3,4</sup> and experimentally<sup>5,6</sup> for single-component materials.

In recent years, more attention has been paid to the multi-component strained layers, in particular the binary (e.g.,  $\text{Si}_{1-x}\text{Ge}_x$ <sup>7,8,9,10,11</sup>) and pseudo-binary (e.g.,  $\text{In}_{1-x}\text{Ga}_x\text{As}$ <sup>12,13,14,15,16,17</sup>) alloys. Since the materials are composed of different kinds of atoms that may not be fully miscible, the compositional inhomogeneities are expected to develop at certain growth conditions. This alloy segregation instability couples with the morphological instability, resulting in the simultaneous modulations of the surface profile and alloy composition during the epitaxial growth.<sup>8,15,16,17</sup> Another important phenomenon of the heteroepitaxial alloy films is the asymmetry of the stability for compressive and tensile layers. For  $\text{Si}_{1-x}\text{Ge}_x$ , films grown under compression were observed to be less stable than those under tension,<sup>7</sup> while for  $\text{In}_{1-x}\text{Ga}_x\text{As}$  the situation is more complicated: Whether compressive or tensile films are more stable seems to depend on the material's growth rate.<sup>13,14,15</sup> Compared with single-component films, there is an extra effect on alloy strain due to composition dependence of the film lattice constant.<sup>18,19</sup> The combination of this compositional strain and the film-substrate misfit strain highly influences the stability behaviors of alloy films.<sup>20,21</sup>

Some theoretical investigations have been carried out in order to understand the morphological instability of strained multi-component films, and most of them focused on the properties and behaviors of growing layers with deposition flux.<sup>20,21,22,23,24,25,26</sup> However, the studies of the static film without deposition<sup>24,27</sup> are much fewer, although the stability of epitaxial films in the absence of growth is also important from both the theoretical and experimental points of view. Using the treatment of thermodynamics, Glas<sup>27</sup> has demonstrated that any strained alloy with a static free surface is unstable due to the interplay of morphological and compositional instabilities. Furthermore, as also pointed out by Glas, this result is valid provided all the evolution mechanisms are possible, and when the physically relevant mechanism is considered, the unstable state derived thermodynamically may not be kinetically accessible. This has been verified in the nonequilibrium and dynamical analysis of Léonard and Desai,<sup>24</sup> where the stability properties of both the non-growing (static) and growing strained alloy films were determined. Stabilization in non-growing film was found to be possible for some parameter values, showing the significance of kinetic evolution process.

In this paper we apply a nonequilibrium, continuum model in order to study the morphological instability and surface decomposition of binary or pseudo-binary strained non-growing alloy films, i.e., films without deposition. The system is assumed to be elastically isotropic and follow the conserved dynamics of phase separation and surface diffusion. Compared with the model of Léonard and Desai<sup>24</sup> and other previous work, here we have two crucial considerations which lead to significantly different stability results. First, due to the fact that the surface phase and bulk phase in a strained film are intimately coupled with each other, we take into account the total free energy of

the system, not just the surface state and energy as used before.<sup>24</sup> Second, the film elastic moduli (both the Young's modulus  $E$  and shear modulus  $\mu$ ) are considered to be composition-dependent, which deeply affects the stability properties. Presenting the linear analysis on early evolution of surface profile and composition, we derive the stability conditions for non-growing film as well as stability diagrams for various material parameters appropriate to realistic systems.

In Sec. II, we describe the continuum model with conserved dynamics and present the mechanical equilibrium equation for the elasticity of this film system. The linear stability analysis is carried out in Sec. III, resulting in the characteristic equation for perturbation growth rate. The results related to the stability conditions and diagrams are shown in Sec. IV, and the discussion and conclusions are presented in Sec. V.

## II. MODEL AND ELASTICITY FORMULATION

We consider a strained alloy system composed of a semi-infinite substrate occupying the region  $z < 0$  and a  $A_{1-X}B_X$  binary or pseudo-binary alloy film in the region  $0 < z < h(x, y)$ , where  $h(x, y)$  represents the surface height variable. The film-substrate interface located at  $z = 0$  is assumed to be planar and remain coherent without generating any misfit dislocation. In this heteroepitaxial system, the misfit strain caused by the difference between the lattice constant of the film  $a_f$  and that of the substrate  $a_s$  is characterized by  $\epsilon = (a_f - a_s)/a_s$ . Thus,  $\epsilon > 0$  or  $< 0$  implies a strained film under compression or tension, respectively. To describe the composition profile of the film, we use a continuous variable  $\phi(\mathbf{r}, t)$  which is defined only for  $z \geq 0$  and is proportional to the local difference in the concentrations of two constituents. Corresponding to an alloy composition  $X$ , its average value  $\bar{\phi}$  is equal to  $2X - 1$ . Here we focus on the symmetric mixture, i.e.,  $X = 1/2$  alloy, for which the spinodal decomposition theory can be well applied, and then we have  $\bar{\phi} = 0$  in what follows. Due to the atomic size difference between  $A$  and  $B$  species, the film lattice parameter  $a_f$  is composition-dependent and the solute expansion coefficient  $\eta = \partial \ln a_f / \partial \phi$ <sup>18,19</sup> is defined to measure the compositional strain.

Assume that the thin film has been grown under ultra-high vacuum condition, e.g., in a molecular-beam epitaxy (MBE) system, and then the evaporation and re-condensation on film surface are negligible. Furthermore, we also neglect the interdiffusion between film and substrate as well as the diffusion and compositional relaxation in the bulk film, since the bulk atomic mobility is much smaller than the mobility at the surface in typical epitaxial growth. Thus, the dynamics of morphological and compositional evolution is dominated by the surface diffusion and surface decomposition processes, and should be conserved.

For the evolution of surface profile, the surface diffusion mechanism leads to

$$\frac{\partial h}{\partial t} = \Gamma_h \sqrt{g} \nabla_s^2 \frac{\delta \mathcal{F}}{\delta h}, \quad (1)$$

while to measure the time-dependence of concentration field at the surface  $\phi(x, y, h(x, y), t) = \phi_s(x, y, t)$ , we apply the conserved dynamics:

$$\frac{\partial \phi}{\partial t} = \Gamma_\phi \nabla^2 \frac{\delta \mathcal{F}}{\delta \phi}. \quad (2)$$

Note that in Eq. (2) there are two ways to study the surface composition fluctuations. The first one<sup>24</sup> is evaluating the free energy  $\mathcal{F}$  at the surface and then calculating the functional differentiation with respect to surface composition field  $\phi_s$ , that is, only considering the surface state. Here we take into account the intimate coupling between surface state and bulk state and use the other way:<sup>26</sup> Apply the total free energy  $\mathcal{F}$  of the whole system to calculate the composition dynamics and then evaluate it at the surface, as has been done in the previous study of surface critical phenomena for spin fluctuations.<sup>28</sup>

In Eqs. (1) and (2),  $\nabla_s^2$  is the surface Laplacian,  $g = 1 + |\nabla h|^2$  represents the determinant of the surface metric, and the kinetic coefficients are denoted as<sup>29</sup>  $\Gamma_h = D_s N_s / k_B T N_v^2$  and  $\Gamma_\phi = \Gamma_h \delta^{-1}$  with  $\delta$  the effective diffusion thickness of surface layer. Here  $D_s$  is the surface diffusivity,  $k_B$  is the Boltzmann constant,  $N_s$  and  $N_v$  are the number densities of atoms per unit surface area and per unit volume, respectively, and  $T$  is the temperature. The total free energy functional  $\mathcal{F}$  consists of three contributions:

$$\mathcal{F} = \mathcal{F}_s + \mathcal{F}_{GL} + \mathcal{F}_{el}. \quad (3)$$

The first contribution  $\mathcal{F}_s$  is the surface energy, which plays a stabilizing role and can be represented by a drumhead model without pinning term:

$$\mathcal{F}_s[h] = \gamma \int d^2 r \sqrt{g}. \quad (4)$$

Here  $\gamma$  is the surface tension, and for simplicity we assume it to be isotropic and composition independent. The second term in r.h.s. of Eq. (3) determines the phase behaviors of binary compounds and is the Ginzburg-Landau functional

$$\mathcal{F}_{\text{GL}}[\phi, h] = \int_{-\infty}^h d^3r \left[ -\frac{r'}{2}\phi^2 + \frac{u}{4}\phi^4 + \frac{c}{2}|\nabla\phi|^2 \right], \quad (5)$$

where the parameters<sup>18</sup>  $r' = k_B(T_c - T)N_v$ ,  $u$  is a temperature independent positive constant, and  $c = k_B T_c N_v a_0^2/2$ , with  $T_c$  the critical temperature of the binary alloy and  $a_0$  the effective interaction distance. For the bulk alloy without elastic strain, when  $T > T_c$  the equilibrium state is homogeneous with  $\phi = 0$ , while for  $T < T_c$  we have the coexistence of two phases  $\phi = \pm\sqrt{r'/u}$ . The last term  $|\nabla\phi|^2$  in Eq. (5) represents the gradient energy that penalizes the sharp compositional changes, and is important for stability analysis: The lack of it leads to a nonphysical divergence for short wavelength mode.<sup>20,22</sup>

The last contribution in Eq. (3) is the elastic free energy functional  $\mathcal{F}_{\text{el}}$ , and is crucial for this stress-driven system. From linear elasticity theory, it can be expressed as

$$\mathcal{F}_{\text{el}}[\phi, \mathbf{u}, h] = \frac{1}{2} \int_{-\infty}^h d^3r S_{ijkl} \sigma_{ij} \sigma_{kl}, \quad (6)$$

where  $\sigma_{ij}$  is the stress tensor and  $S_{ijkl}$  is the elastic compliance tensor with the form  $S_{ijkl} = \delta_{ik}\delta_{jl}(1+\nu)/E - \delta_{ij}\delta_{kl}\nu/E$  for isotropic systems (subscripts  $i, j, k$ , or  $l = x, y, z$ ). Generally, the elastic constants (Young's modulus  $E$ , shear modulus  $\mu$ , and Poisson ratio  $\nu$ ) are dependent of the local composition, and here we consider this dependence to first order, that is,

$$\begin{aligned} E &= E_0(1 + E_1^*\phi), \\ \mu &= \mu_0(1 + \mu_1^*\phi), \end{aligned} \quad (7)$$

and  $\nu = E/2\mu - 1$ . In this paper we take the system as being elastically isotropic, and neglect the difference in the average elastic constants ( $E_0$ ,  $\mu_0$ , and  $\nu_0 = E_0/2\mu_0 - 1$ ) between film and substrate. This is appropriate for systems with substrate and film having similar elastic constants.

To determine the elastic energy (6), we need to get the solution for the displacement vector  $\mathbf{u}$  which satisfies mechanical equilibrium

$$\partial_j \sigma_{ij} = 0 \quad (8)$$

in the whole film/substrate system. According to Hooke's law for isotropic system, the linear stress tensor is expressed as

$$\sigma_{ij} = 2\mu \left[ \frac{\nu}{1-2\nu} u_{ll} \delta_{ij} + u_{ij} - \frac{1+\nu}{1-2\nu} (\epsilon + \eta\phi) \delta_{ij} \right], \quad (9)$$

with the presence of misfit strain  $\epsilon$  and composition strain  $\eta\phi$ , where the linear strain tensor  $u_{ij}$  is given by

$$u_{ij} = (\partial_i u_j + \partial_j u_i)/2. \quad (10)$$

The boundary conditions are needed to solve the above mechanical equilibrium equation. At the free surface of the film, i.e., at  $z = h(x, y)$ , we have

$$\sigma_{ij}^f n_j = 0 \quad (11)$$

due to the negligible pressure on the film surface. Here  $n_j$  is the unit vector normal to the surface. Since the film-substrate interface at  $z = 0$  remains coherent, we get the continuous conditions for both stress and displacement tensors:

$$\sigma_{ij}^f = \sigma_{ij}^s \quad \text{and} \quad u_i^f = u_i^s, \quad (12)$$

where superscripts  $f$  and  $s$  refer to the film and substrate, respectively. Finally, the strains far from the interface, that is, for  $z \rightarrow -\infty$ , are expected to decay to zero:

$$u_i^s \rightarrow 0 \quad \text{and} \quad u_{ij}^s \rightarrow 0. \quad (13)$$

### III. LINEAR STABILITY ANALYSIS

In order to determine the stability properties of this non-growing strained alloy system, we apply the linear analysis on evolution equations (1) and (2) with the use of formulae (3)–(13). For a general variable  $\xi$ , which could be displacement  $u_i$ , composition field  $\phi$ , or height variable  $h$ , its Fourier expansion yields

$$\xi = \bar{\xi} + \sum_{\mathbf{q}} \hat{\xi}(\mathbf{q}, z, t) e^{i(q_x x + q_y y)}, \quad (14)$$

with small perturbations  $\hat{\xi}$  around the basic state  $\bar{\xi}$  which corresponds to a planar film with fixed thickness  $h_0 = \bar{h}$  and uniform composition  $\bar{\phi} = 0$ . Note that in Eq. (14) when  $\xi$  denotes the height variable  $h$ ,  $\hat{\xi}$  is in fact  $\hat{h}(\mathbf{q}, t)$ . The basic-state solution<sup>20,24</sup> for the film leads to  $\bar{u}_x^f = \bar{u}_y^f = 0$ ,  $\bar{u}_z^f = \bar{u}z$  with  $\bar{u} = \bar{u}_{zz}^f = \epsilon(1 + \nu_0)/(1 - \nu_0)$ ,  $\bar{\sigma}_{xx}^f = \bar{\sigma}_{yy}^f = \bar{\sigma} = -2\mu_0\bar{u}$ , and other stress and strain tensors ( $\bar{u}_{ij}^f$ ,  $\bar{\sigma}_{ij}^f$ ) to be zero. For the substrate, the basic state is unstrained and then  $\bar{u}_i^s = 0$  and  $\bar{u}_{ij}^s = \bar{\sigma}_{ij}^s = 0$  ( $i, j = x, y, z$ ).

The mechanical equilibrium equation (8) with boundary conditions (11)–(13) can be solved to first order  $O(\hat{h}, \hat{\phi})$  using the above expansion (14). Here we use the detailed solutions given by Léonard and Desai<sup>24</sup>, where a crucial step is to introduce a new variable  $W$  with

$$\nabla^2 W = \phi, \quad (15)$$

or equivalently,  $(\partial_z^2 - q^2)\hat{W} = \hat{\phi}$  with  $q^2 = q_x^2 + q_y^2$ . After substituting the solutions in the free energy functional (3)–(6) and then in the dynamical equations (1) and (2), we can obtain the linearized evolution equations for morphological and compositional perturbations  $\hat{h}$  and  $\hat{\phi}$  to determine the stability of the system.

What we are interested in is the behavior of perturbations for the stressed film without deposition. The fluctuations of alloy composition mainly occur at the surface  $z = h(x, y)$  due to the surface relaxation process, and should attenuate along the vertical direction  $z$  as the surface/bulk coupling weakens with the increasing distance from the surface and the bulk mobility is very small. Thus, the bulk compositional perturbation  $\hat{\phi}_b$  caused by the free surface disturbance is hypothesized to decay as

$$\hat{\phi}_b = \hat{\phi}_s e^{-\kappa(h_0 - z)}, \quad (16)$$

with the corresponding  $\hat{W} = \hat{\phi}_s e^{-\kappa(h_0 - z)}/(\kappa^2 - q^2)$ . This exponential form is for the early evolution regime and similar to that used in previous work.<sup>24,27</sup> The parameter  $\kappa$  in Eq. (16) is equal to  $1/b$ , with  $b$  the vertical length scale of compositional perturbation caused by free surface. Due to the negligible atomic mobility in the bulk and guided by the fact that the vertical morphological perturbation is very small compared with the lateral variation, one can assume  $b \ll \lambda$ , where  $\lambda \sim 1/q$  is the typical lateral wavelength of surface modulation. Therefore, for the range of  $q$  that corresponds to typical surface structure, we have

$$\kappa \gg q \quad (17)$$

in Eq. (16).

Using the solutions of mechanical equilibrium equation and the assumptions (16) and (17), we have derived the dynamical equations for  $\hat{h}$  and  $\hat{\phi}_s$ . To first order of the perturbations, they are (in nondimensional form)

$$\partial \hat{h}^* / \partial \tau = (\epsilon^{*2} k^3 - \gamma^* k^4) \hat{h}^* - \frac{k^2}{1 + \nu_0} \left[ \epsilon^* \eta^* + \frac{2E_1^* - (1 + \nu_0)\mu_1^*}{2(1 - \nu_0)} \epsilon^{*2} \right] \hat{\phi}_s^*, \quad (18)$$

and

$$\begin{aligned} \partial \hat{\phi}_s^* / \partial \tau = & \frac{k^3}{1 - \nu_0} \left[ (1 - 2\nu_0) \epsilon^* \eta^* + (2E_1^* - (1 + \nu_0)\mu_1^*) \epsilon^{*2} \right] \hat{h}^* \\ & - k^2 \left[ k^2 \pm 1 + \frac{8E_1^* - 5(1 + \nu_0)\mu_1^*}{2(1 - \nu_0^2)} \epsilon^* \eta^* \right] \hat{\phi}_s^*, \end{aligned} \quad (19)$$

where the “ $\pm$ ” sign corresponds to the cases in which the alloy is above (“+”) or below (“−”) the effective critical temperature  $T_c^{\text{eff}}$  defined by

$$T_c^{\text{eff}} = T_c - \frac{2E_0}{1 - \nu_0} \frac{\eta^2}{k_B N_v}, \quad (20)$$

which is the same as the spinodal temperature of alloys with coherency stress derived by Cahn.<sup>18</sup>

Here we have rescaled the variables and parameters to make the equations nondimensional, using a characteristic length scale

$$l_0 = \left( \frac{|r|}{c} \right)^{-1/2}, \quad (21)$$

which is the typical width of domain interfaces, and time scale

$$\tau_0 = \left( \Gamma_\phi \frac{r^2}{c} \right)^{-1}, \quad (22)$$

with

$$r = r' - 2E_0\eta^2/(1 - \nu_0) = k_B(T_c^{\text{eff}} - T)N_v, \quad (23)$$

as well as the transformations:

$$\begin{aligned} k &= ql_0, \\ \tau &= t/\tau_0, \\ \hat{h}^* &= h/l_0, \\ \hat{\phi}_s^* &= \hat{\phi}_s, \\ \gamma^* &= \frac{l_0}{c}\gamma, \\ \epsilon^* &= \left[ \frac{2E_0}{|r|} \left( \frac{1 + \nu_0}{1 - \nu_0} \right) \right]^{1/2} \epsilon, \\ \eta^* &= \left[ \frac{2E_0}{|r|} \left( \frac{1 + \nu_0}{1 - \nu_0} \right) \right]^{1/2} \eta. \end{aligned} \quad (24)$$

In the early time regime of the perturbation's evolution, the growth rates of morphological and compositional perturbations, i.e.,  $\sigma_h$  and  $\sigma_\phi$ , are defined through  $\hat{h}^* = \hat{h}_0 \exp(\sigma_h \tau)$  and  $\hat{\phi}_s^* = \hat{\phi}_0 \exp(\sigma_\phi \tau)$ , respectively. In general cases (e.g., both  $\epsilon^*$  and  $\eta^*$  are nonzero) two dynamical equations (18) and (19) couple with each other, which leads to the joint stability or instability of surface morphology and composition, that is,  $\sigma_h = \sigma_\phi = \sigma$ . Therefore, from Eqs. (18) and (19) we can obtain the characteristic equation for the perturbation growth rate  $\sigma$ :

$$\begin{aligned} &(\sigma + \gamma^* k^4 - \epsilon^{*2} k^3) \left[ \sigma + k^2 \left( k^2 \pm 1 + \frac{8E_1^* - 5(1 + \nu_0)\mu_1^*}{2(1 - \nu_0^2)} \epsilon^* \eta^* \right) \right] \\ &+ \frac{k^5}{2(1 + \nu_0)(1 - \nu_0)^2} \left[ (1 - 2\nu_0)\epsilon^* \eta^* + (2E_1^* - (1 + \nu_0)\mu_1^*)\epsilon^{*2} \right] \\ &\times \left[ 2(1 - \nu_0)\epsilon^* \eta^* + (2E_1^* - (1 + \nu_0)\mu_1^*)\epsilon^{*2} \right] = 0, \end{aligned} \quad (25)$$

where the “+” (“−”) sign corresponds to  $T > T_c^{\text{eff}}$  ( $T < T_c^{\text{eff}}$ ). The real part of  $\sigma$  determines the stability properties of the system: For  $\text{Re}(\sigma) > 0$ , the film is jointly unstable to morphological instability and alloy decomposition instability at the surface, while if  $\text{Re}(\sigma) < 0$  is fulfilled for all the wavenumbers  $k$ , both the morphological and compositional modulations are suppressed. When  $\text{Re}(\sigma) > 0$  and  $\text{Im}(\sigma) \neq 0$ , the instability is oscillatory. In the following calculations, we first (Sec. IV A and IV B) focus on the real part of  $\sigma$  for each of the solutions of Eq. (25), and use the largest one (with respect to all evolution modes  $k$ ) to determine the regions of instability. Within the unstable region, the imaginary part is then computed (Sec. IV C) to determine the regions of oscillatory instability.

Note that in Eq. (25), quantities  $k$ ,  $\gamma^*$ ,  $\epsilon^*$ ,  $\eta^*$  depend on temperature via the coefficient  $r$  (see Eqs. (23), (21), and (24)). The temperature dependence of the system's stability can be made explicit by rewriting Eq. (25) in a dimension-full manner, which is

$$\begin{aligned} &\left[ \Omega\tau_0 + \frac{c^{3/2}}{|r|^{5/2}} \left( \gamma q^4 - 2E_0 \frac{1 + \nu_0}{1 - \nu_0} \epsilon^2 q^3 \right) \right] \\ &\times \left[ \Omega\tau_0 + \frac{c}{r^2} q^2 \left( -r + cq^2 + \frac{E_0}{(1 - \nu_0)^2} (8E_1^* - 5(1 + \nu_0)\nu_1^*)\epsilon\eta \right) \right] \end{aligned}$$

$$\begin{aligned}
& + \frac{c^{5/2}}{|r|^{9/2}} \frac{2E_0^2(1+\nu_0)}{(1-\nu_0)^4} q^5 [(1-2\nu_0)\epsilon\eta + (2E_1^* - (1+\nu_0)\mu_1^*)\epsilon^2] \\
& \times [2(1-\nu_0)\epsilon\eta + (2E_1^* - (1+\nu_0)\mu_1^*)\epsilon^2] = 0.
\end{aligned} \tag{26}$$

Thus, in this characteristic equation for the perturbation growth rate  $\sigma$  ( $= \Omega\tau_0$ ), the temperature dependence enters only through the quantity  $r$  which is linearly dependent on  $T$  as given by Eq. (23). Even though the characteristic time scale  $\tau_0$  depends on temperature (Eq. (22)), this dependence does not have any effect on stability boundaries.

#### IV. RESULTS

From Eqs. (18)–(25), the stability property of the strained film depends on material parameters  $\epsilon^*$ ,  $\eta^*$ ,  $E_1^*$ ,  $\mu_1^*$ ,  $\gamma^*$ , and  $\nu_0$ . In the following we give the results of film stability for the cases of composition independent and dependent elastic constants, as well as different conditions of misfit and compositional strains.

##### A. Composition-independent elastic moduli ( $E_1^* = \mu_1^* = 0$ )

When ignoring the dependence of elastic constants on the local composition, we have  $E = E_0$ ,  $\mu = \mu_0$ , and  $\nu = \nu_0$  from Eq. (7), and the derived evolution equations for perturbations  $\hat{h}^*$  and  $\hat{\phi}_s^*$  as well as the characteristic equation for  $\sigma$  are the same as Eqs. (18), (19) and (25) after setting  $E_1^* = \mu_1^* = 0$ .

When  $\epsilon^* = \eta^* = 0$ , that is, neither misfit strain nor compositional strain exists in the film, the dynamical equations for  $\hat{h}^*$  and  $\hat{\phi}_s^*$  decouple, with different perturbation growth rate:

$$\begin{aligned}
\sigma_h &= -\gamma^* k^4, \\
\sigma_\phi &= \begin{cases} -k^4 - k^2, & \text{if } T > T_c^{\text{eff}} \\ -k^4 + k^2, & \text{if } T < T_c^{\text{eff}} \end{cases}
\end{aligned} \tag{27}$$

which recovers the results obtained by Léonard and Desai.<sup>24</sup> Thus, the surface morphology is always stable and the compositional stability is similar to that of bulk alloy: For  $T > T_c^{\text{eff}}$  ( $= T_c$ , when  $\eta = 0$ ) the system is stable, while for  $T < T_c^{\text{eff}}$  spinodal decomposition occurs for long wavelengths ( $k < 1$ ). For the case of zero misfit but nonzero solute expansion coefficient, i.e.,  $\epsilon^* = 0$  and  $\eta^* \neq 0$ , the dispersion relations are the same as (27). Note that the compositional perturbation rate  $\sigma_\phi$  obtained here is different from that of the previous work (see Eq. (44) in Ref. 24).

When  $\epsilon^* \neq 0$  and  $\eta^* = 0$ , corresponding to nonzero misfit stress but zero solute stress, our results yield:

$$\begin{aligned}
\sigma_h &= \epsilon^{*2} k^3 - \gamma^* k^4, \\
\sigma_\phi &= \begin{cases} -k^4 - k^2, & \text{if } T > T_c \\ -k^4 + k^2, & \text{if } T < T_c \end{cases}
\end{aligned} \tag{28}$$

where the Asaro-Tiller-Grinfeld instability for morphology<sup>1,2</sup> is recovered, as also shown in the model of Léonard and Desai.

For more general case of  $\epsilon^* \neq 0$  and  $\eta^* \neq 0$ , that is, the strains generated by both the lattice mismatch and compositional nonuniformity are nonzero and coupled, we have a quadratic equation for the common perturbation growth rate  $\sigma$ :

$$\sigma^2 + a_1\sigma + a_0 = 0, \tag{29}$$

with the roots  $\sigma = (-a_1 \pm \sqrt{a_1^2 - 4a_0})/2$  and coefficients

$$\begin{aligned}
a_1 &= \gamma^* k^4 - \epsilon^{*2} k^3 + k^2(k^2 \pm 1), \\
a_0 &= k^2(k^2 \pm 1)(\gamma^* k^4 - \epsilon^{*2} k^3) + \frac{1-2\nu_0}{1-\nu_0^2} \epsilon^{*2} \eta^{*2} k^5.
\end{aligned} \tag{30}$$

Usually the Poisson ratio  $\nu_0$  lies in the range from 1/4 to 1/3. Consequently, for  $T < T_c^{\text{eff}}$  (bottom sign “−” in Eq. (30)), we have  $a_1 < 0$  and  $a_0 > 0$  when the wavenumber is very small, i.e.,  $k \ll 1$ , corresponding to the solution  $\text{Re}(\sigma) > 0$ . Then the instabilities of surface morphological and compositional profiles are expected to appear simultaneously below the effective critical temperature.

For  $T > T_c^{\text{eff}}$ , the stability properties are more complicated and we present the analytic results as follows. If  $\gamma^{*2} > \gamma^* + 1$  (i.e.,  $\gamma^* > (1 + \sqrt{5})/2$ ), the stability condition for this strained film is

$$\epsilon^{*2} < 2(1 + \gamma^*)^{1/2} \quad \text{and} \quad \eta^{*2} > \eta_0^{*2}, \quad (31)$$

with  $\eta_0^{*2} = (1 - \nu_0^2)/(1 - 2\nu_0)$ . Otherwise, if  $\gamma^{*2} < \gamma^* + 1$  (i.e.,  $0 < \gamma^* < (1 + \sqrt{5})/2$ ), the system is stable when

$$\epsilon^{*2} < 2\gamma^* \quad \text{and} \quad \eta^{*2} > \eta_0^{*2}, \quad (32)$$

or

$$2\gamma^* < \epsilon^{*2} < 2(1 + \gamma^*)^{1/2} \quad \text{and} \quad \eta^{*2} > \eta_0^{*2} \left[ 1 - \frac{\epsilon^{*2}(9\gamma^{*2} - 2\epsilon^{*4}) - 2(\epsilon^{*4} - 3\gamma^{*2})^{3/2}}{27\gamma^{*2}\epsilon^{*2}} \right]. \quad (33)$$

Therefore, in this stress-driven epitaxial system the instability of both morphology and composition could also occur above the strained spinodal temperature  $T_c^{\text{eff}}$  and for large misfit  $\epsilon^*$  or small solute coefficient  $\eta^*$ . This result is very different from the bulk alloy where only below the critical temperature, can the spinodal decomposition be present. This instability is due to the coupling of morphological and compositional undulations, as pointed out by Glas<sup>27</sup> from the thermodynamic point of view.

The corresponding stability boundary in the  $\epsilon^*$ - $\eta^*$  space is shown for  $\nu_0 = 1/4$  and different values of  $\gamma^*$  in Fig. 1 (thick lines). The stability boundary for  $\gamma^* = 5$  corresponds to the case of  $\gamma^{*2} > \gamma^* + 1$  and then is determined by Eq. (31), while for  $\gamma^* = 0.5$  the conditions (32) and (33) are used. The stabilizing effect of surface energy can be seen directly from the figure, where the stable region is enlarged with the increasing value of surface tension  $\gamma^*$ . The stability diagram here is symmetric with respect to the sign of misfit  $\epsilon^*$  since we have assumed the composition independence of elastic moduli in Fig. 1.

### B. Composition-dependent elastic moduli ( $E_1^* \neq 0$ , $\mu_1^* \neq 0$ )

More interesting and richer results are obtained for the cases of composition-dependent elastic constants with  $E_1^* \neq 0$  and  $\mu_1^* \neq 0$ , where the coupling of misfit strain, solute strain and composition dependence of elastic moduli can highly affect the behaviors of perturbation growth.

For the lattice matched films, that is,  $\epsilon^* = 0$  with  $\eta^*$  arbitrary, the morphological and compositional degrees of freedom decouple, as obtained from dynamical equations (18) and (19). The perturbation growth rates  $\sigma_h$  and  $\sigma_\phi$  also obey Eq. (27), corresponding to the stability properties the same as that of  $E_1^* = \mu_1^* = 0$ . However, when lattice misfit exists, i.e.,  $\epsilon^* \neq 0$ , the composition dependence of elastic constants leads to substantially different results. In the absence of atomic size difference ( $\eta^* = 0$ ), the dynamical equations for  $\hat{h}^*$  and  $\hat{\phi}_s^*$  remain coupled, which is qualitatively different from the case shown in Eq. (28) for composition independent elastic moduli. The coupled perturbation growth rate  $\sigma$  is then governed by a quadratic equation of the form similar to Eq. (29)

$$\sigma^2 + a_1\sigma + a_0 = 0,$$

but with different coefficient  $a_0$ :

$$\begin{aligned} a_1 &= \gamma^*k^4 - \epsilon^{*2}k^3 + k^2(k^2 \pm 1), \\ a_0 &= k^2(k^2 \pm 1)(\gamma^*k^4 - \epsilon^{*2}k^3) + \frac{[2E_1^* - (1 + \nu_0)\mu_1^*]^2}{2(1 + \nu_0)(1 - \nu_0)^2} \epsilon^{*4}k^5. \end{aligned} \quad (34)$$

When  $T < T_c^{\text{eff}}$ , it is easy to show that  $\text{Re}(\sigma) > 0$  for  $k \ll 1$  and then the system is unstable, while for  $T > T_c^{\text{eff}}$  the film can be stable for certain values of misfit  $\epsilon^*$ , as specified in the following stability conditions: If  $\gamma^{*2} > \gamma^* + 1$ , the stability occurs for

$$\chi^{-1} < \epsilon^{*2} < 2(1 + \gamma^*)^{1/2}, \quad (35)$$

with

$$\chi = \frac{[2E_1^* - (1 + \nu_0)\mu_1^*]^2}{2(1 + \nu_0)(1 - \nu_0)^2}; \quad (36)$$

while for  $\gamma^{*2} < \gamma^* + 1$ , there are two regions of stability. In the first one,

$$\chi^{-1} < \epsilon^{*2} < 2\gamma^*, \quad (37)$$

is fulfilled. In the other, four conditions have to be fulfilled:

$$(i) 2\gamma^* < \epsilon^{*2} < 2(1 + \gamma^*)^{1/2}, \quad (38)$$

$$(ii) \gamma^* > \frac{4}{9}\chi^{-1}, \quad (39)$$

$$(iii) \gamma^* > \frac{\epsilon^{*2}}{3(3\chi\epsilon^{*2}/2 - 1)^{1/2}}, \quad (40)$$

and (iv)

$$\begin{aligned} & \frac{2}{3}\chi^{-1} < \epsilon^{*2} < \frac{8}{9}\chi^{-1}, \\ & \text{or} \\ & \epsilon^{*2} > \frac{8}{9}\chi^{-1}, \text{ and } \gamma^{*2} > \frac{\epsilon^{*4}}{2} \left[ \left( \frac{\chi}{2} \right)^{1/2} \left( \frac{9}{2}\chi\epsilon^{*2} - 4 \right)^{3/2} \epsilon^* - 3 \left( \frac{3}{2}\chi\epsilon^{*2} - 1 \right)^2 + 1 \right], \\ & \text{or} \\ & \epsilon^{*2} > \frac{8}{9}\chi^{-1}, \text{ and } \gamma^{*2} < \frac{\epsilon^{*4}}{2} \left[ - \left( \frac{\chi}{2} \right)^{1/2} \left( \frac{9}{2}\chi\epsilon^{*2} - 4 \right)^{3/2} \epsilon^* - 3 \left( \frac{3}{2}\chi\epsilon^{*2} - 1 \right)^2 + 1 \right]. \end{aligned} \quad (41)$$

The stability diagram of  $|\epsilon^*|$  vs  $\gamma^*$  corresponding to Eqs. (35)–(40) is plotted in Fig. 2, where the parameters  $\nu_0 = 1/4$ ,  $E_1^* = -0.4$ , and  $\mu_1^* = -0.1$  are chosen. One can see from the diagram that in the absence of compositional strain but with the composition dependence of elastic constants, the system above the effective critical temperature can be stabilized for intermediate magnitudes of misfit  $\epsilon^*$  and large enough effective surface tension  $\gamma^*$ .

For the most general case  $\epsilon^* \neq 0$ ,  $\eta^* \neq 0$  and  $E_1^* \neq 0$ ,  $\mu_1^* \neq 0$ , corresponding to the lattice mismatched and compositionally stressed film with composition-dependent elastic constants, the coupled dynamical equations are described in (18) and (19), with joint perturbation growth rate  $\sigma$  given by Eq. (25). The characteristic equation (25) is in fact quadratic, with coefficients

$$\begin{aligned} a_1 &= \gamma^* k^4 - \epsilon^{*2} k^3 + k^2 [k^2 \pm 1 + \beta \epsilon^* \eta^*], \\ a_0 &= k^2 (\gamma^* k^4 - \epsilon^{*2} k^3) [k^2 \pm 1 + \beta \epsilon^* \eta^*] \\ &+ \frac{k^5}{2(1 + \nu_0)(1 - \nu_0)^2} \left[ (1 - 2\nu_0)\epsilon^* \eta^* + \alpha \epsilon^{*2} \right] \left[ 2(1 - \nu_0)\epsilon^* \eta^* + \alpha \epsilon^{*2} \right], \end{aligned} \quad (42)$$

with the parameters

$$\begin{aligned} \alpha &= 2E_1^* - (1 + \nu_0)\mu_1^*, \\ \beta &= \frac{8E_1^* - 5(1 + \nu_0)\mu_1^*}{2(1 - \nu_0^2)}. \end{aligned} \quad (43)$$

The stability conditions can be derived by studying the real part of the solutions  $\sigma = (-a_1 \pm \sqrt{a_1^2 - 4a_0})/2$ , and we present the analytic results below for both  $T > T_c^{\text{eff}}$  and  $T < T_c^{\text{eff}}$ .

The stable epitaxial film should first fulfill:

$$\beta \epsilon^* \eta^* \pm 1 > 0, \quad (44)$$

and then similar to the other cases, the conditions for  $\gamma^{*2} > \gamma^* + 1$  or  $\gamma^{*2} < \gamma^* + 1$  are different. For  $\gamma^{*2} > \gamma^* + 1$ , the stability conditions are

$$\epsilon^{*4} < 4(\gamma^* + 1)(\beta \epsilon^* \eta^* \pm 1), \quad (45)$$

and

$$\begin{aligned} & \Delta < 0, \\ & \text{or} \\ & \Delta > 0 \quad \text{and} \quad \eta^* > \frac{-\rho \epsilon^* + \Delta^{1/2}}{4(1 - \nu_0)(1 - 2\nu_0)}, \\ & \text{or} \\ & \Delta > 0 \quad \text{and} \quad \eta^* < \frac{-\rho \epsilon^* - \Delta^{1/2}}{4(1 - \nu_0)(1 - 2\nu_0)}, \end{aligned} \quad (46)$$



where

$$\begin{aligned}\rho &= -2E_1^* + (1 + \nu_0)(2 - \nu_0)\mu_1^*, \\ \Delta &= [\rho^2 - 8(1 - \nu_0)(1 - 2\nu_0)\alpha^2] \epsilon^{*2} \pm 16(1 + \nu_0)(1 - \nu_0)^3(1 - 2\nu_0).\end{aligned}\quad (47)$$

On the other hand, for  $\gamma^{*2} < \gamma^* + 1$  the system is stable only when the following conditions are fulfilled:

$$\epsilon^{*4} < 4\gamma^{*2}(\beta\epsilon^*\eta^* \pm 1), \quad (48)$$

as well as all the conditions in Eq. (46), or

$$\begin{aligned}4\gamma^{*2}(\beta\epsilon^*\eta^* \pm 1) &< \epsilon^{*4} < 4(\gamma^* + 1)(\beta\epsilon^*\eta^* \pm 1), \\ \text{and} \\ \left[ \frac{1 - 2\nu_0}{1 - \nu_0^2} \eta^{*2} + \frac{\rho}{2(1 + \nu_0)(1 - \nu_0)^2} \epsilon^*\eta^* + \frac{\alpha^2}{2(1 + \nu_0)(1 - \nu_0)^2} \epsilon^{*2} \mp 1 \right] \epsilon^{*2} \\ + \frac{\epsilon^{*2}}{27\gamma^{*2}} [9\gamma^{*2}(\beta\epsilon^*\eta^* \pm 1) - 2\epsilon^{*4}] - \frac{2}{27\gamma^{*2}} [\epsilon^{*4} - 3\gamma^{*2}(\beta\epsilon^*\eta^* \pm 1)]^{3/2} &> 0.\end{aligned}\quad (49)$$

Note that in Eqs. (42), (44), (45), (47)–(49), the top sign applies when the temperature  $T$  is above the effective critical temperature  $T_c^{\text{eff}}$ , and the bottom sign corresponds to  $T < T_c^{\text{eff}}$ .

The stability diagrams can be calculated according to above results (44)–(49). Here we use two sets of parameters (1 and 2) to plot the stability diagrams of  $T > T_c^{\text{eff}}$  and  $T < T_c^{\text{eff}}$ , as shown in Figs. 3–6. For the first set (Set 1, used in Figs. 3 and 5), where all the material parameters (e.g.,  $T_c$ ,  $\gamma$ ,  $a_f$ ,  $N_v$ , and elastic constants) are chosen to qualitatively represent the SiGe alloy, we have  $\nu_0 = 1/4$  and  $\gamma^* = 5$  obtained from Eq. (24), and assume that  $E_1^* = -0.4$ ,  $\mu_1^* = -0.1$ . The second set 2 is expected to qualitatively represent the InGaAs alloy and applies to Figs. 4 and 6, where we choose  $\nu_0 = 1/3$ ,  $\gamma^* = 3.5$ ,  $E_1^* = -0.25$ , and  $\mu_1^* = -0.5$ .

Compared to symmetric diagram Fig. 1 for  $E_1^* = \mu_1^* = 0$ , Figs. 3–6 exhibit the asymmetry for compressive and tensile layers, i.e., the stability depends on the sign of misfit  $\epsilon^*$ , which is one of the major consequence of local composition dependence of elastic constants. In Figs. 3 and 5, corresponding to parameters of Set 1 (similar to the case of SiGe), the stabilization mainly occurs under tensile strain ( $\epsilon^* < 0$ ) and the stable regions increase with larger value of  $\eta^*$ , while for compressive films the instability can not be suppressed for most of the parameter values, especially for  $T < T_c^{\text{eff}}$ . In contrast, the InGaAs-like parameters of Set 2 lead to opposite asymmetry: Larger part of stable region is found in positive misfit  $\epsilon^*$ , and layers subject to tensile strain exhibit less stability, as shown in Figs. 4 and 6.

The other important effect of composition-dependent elastic moduli is on the system below effective critical temperature  $T_c^{\text{eff}}$ . For all the other cases described above, including the ones for  $E_1^* \neq 0$  and  $\mu_1^* \neq 0$  but with one of  $\epsilon^*$  and  $\eta^*$  equal to zero, the compositional profiles for  $T < T_c^{\text{eff}}$  are unstable, in agreement with the usual expectation that the strained alloy near 50–50 mixture should exhibit decomposition and phase segregation below the coherent spinodal temperature  $T_c^{\text{eff}}$ . However, the coupling of all the factors of misfit strain, solute strain and composition-dependent moduli causes different and new effects. As shown in Figs. 5 and 6 when all the variables  $\epsilon^*$ ,  $\eta^*$ ,  $E_1^*$  and  $\mu_1^*$  are nonzero, the film below  $T_c^{\text{eff}}$  can also be stable for certain range of parameters. That is, it is possible to suppress the surface decomposition even for  $T < T_c^{\text{eff}}$  due to the coupling effects in this heteroepitaxial system.

### C. Oscillatory instability ( $\text{Im}(\sigma) \neq 0$ )

When the system corresponds to the unstable parameters region of stability diagram, that is,  $\text{Re}(\sigma) > 0$ , the imaginary part of  $\sigma$  determines whether the onset of this instability is steady ( $\text{Im}(\sigma) = 0$ ) or oscillatory ( $\text{Im}(\sigma) \neq 0$ ). The occurrence of oscillatory instability has been found in the study of directional solidification for stressed solid<sup>32</sup> and the growing process of alloy thin films,<sup>20</sup> and been attributed to the phase difference between surface morphology and composition field, induced by nonlocal elastic stresses.

We calculate the imaginary part of perturbation growth rate  $\sigma$  through characteristic equation (25). If for a certain wavenumber  $k$ , we have both  $\text{Re}(\sigma) > 0$  and  $\text{Im}(\sigma) \neq 0$ , the oscillatory instability may occur. The results for  $\epsilon^* \neq 0$ ,  $\eta^* \neq 0$ , and  $T > T_c^{\text{eff}}$ , corresponding to the parameters range of most experiments on strained films, are shown in Figs. 1, 3, and 4 with the thin dashed or dotted boundary curves. For the case of composition independent elastic moduli, as shown in Fig. 1, the oscillatory unstable regions are symmetric with respect to misfit and more regular. Large solute coefficient  $\eta^*$  favours the occurrence of oscillatory instability, and if misfit  $\epsilon^*$  is large enough, the oscillatory instability is obtained when  $\eta^*$  exceeds a fixed value  $\eta_0^* = [(1 - \nu_0^2)/(1 - 2\nu_0)]^{1/2}$ , which can be derived analytically.

When the elastic constants are composition dependent, *i.e.*  $E_1^* \neq 0$  and  $\mu_1^* \neq 0$ , the oscillatory regions are asymmetric and irregular (see Figs. 3 and 4). Note that in these parameter regions of oscillatory instability, steady instability can also exist (but for different mode  $k$ ), and the competition between these two kinds of unstable modes determines the surface profile. When oscillatory modes dominate or coexist with steady modes, the surface disturbance is expected to propagate laterally, with the phenomenon that one side of the surface bump will grow faster than the other side.<sup>32</sup>

## V. DISCUSSION AND CONCLUSIONS

Our calculations above have shown that the stability problem of free alloy film surface under both morphological and compositional strains is essentially a nonequilibrium and dynamical problem even for static films, *i.e.*, in the absence of growth. Although in the sense of thermodynamics and equilibrium, it has been demonstrated that the instability can appear in any stressed alloy with free surface,<sup>27</sup> the physically based choice of non-equilibrium evolution dynamics leads to different conclusion that the system can be stabilized for certain values of parameters. As shown in Figs. 1–6, the joint instability can be suppressed by large enough compositional strain ( $\eta^*$ ), which has also been found for growing films in the film-vapor local equilibrium model of Guyer and Voorhees<sup>20</sup> as well as in the dynamical model of Spencer *et al.*<sup>22</sup> with unequal atomic mobilities for different alloy constituents.

In the previous work<sup>20,22,24</sup> this stabilization of compositional stresses would be overcome by larger magnitude of misfit  $\epsilon^*$ , while in our results similar phenomenon occurs for  $\epsilon^*$  values far from zero, but the other parts of stability diagrams are more complicated. In Fig. 4 (with parameters of Set 2 and  $T > T_c^{\text{eff}}$ ) and Figs. 5 and 6 for  $T < T_c^{\text{eff}}$ , when the magnitude of misfit  $\epsilon^*$  is close to the minimum of the stability boundary and is made smaller, then higher value of  $\eta^*$  (related to larger compositional strain) is needed to suppress the instability, and for parameters of Set 1 with  $T > T_c^{\text{eff}}$  (Fig. 3) the stable regions are much more irregular, due to the combination of misfit and compositional strains as well as composition-dependent elastic moduli. Even for the case of composition-independent moduli, the results here (shown in Fig. 1) are different from before. For sufficiently large  $\eta$ , the nonphysical short wavelength divergence<sup>20,22</sup> is avoided due to the inclusion of gradient energy and the return of instability<sup>24</sup> is not found here due to the consideration of coupling between surface and bulk phases.

The introduction of composition dependence of alloy elastic constants, which makes the effective elastic effects nonlocal, leads to the presence of asymmetry in the stability of films under compression or tension. Some experiments have tested this misfit sign dependence. Although these observations are all for the growing films, they can still be helpful to check our theoretical results for films without deposition. Our calculations using parameters similar to that of SiGe (shown in Figs. 3 and 5) exhibit the preference of stability for tensile layers, consistent with the experimental findings of Xie *et al.*<sup>7</sup> Various experiments<sup>13,14,15</sup> indicated that the way of asymmetry for InGaAs alloys depends on the materials deposition rate, while our results in Figs. 4 and 6 with a specific selection of parameters (Set 2) suggest that the compressive layers are more stable for non-growing film.

The simultaneous interaction of misfit strain, solute strain and composition-dependent elastic constants makes the stability possible even for  $T < T_c^{\text{eff}}$ , which is not possible in the absence of any one of them. The corresponding diagrams are shown in Figs. 5 and 6. This phenomenon is very different from what we expect, since in usual bulk strained alloy the spinodal decomposition always occurs below  $T_c^{\text{eff}}$ .<sup>18</sup> The related experiments are lacking since most of the epitaxial experiments are carried out above the effective critical temperature  $T_c^{\text{eff}}$ .

Note that although in the above analysis, we have distinguished the stability results and diagrams into two temperature regimes  $T > T_c^{\text{eff}}$  and  $T < T_c^{\text{eff}}$ , in each regime the stability properties are still temperature dependent. This can be seen from our theoretical diagrams (Figs. 1 – 6) as well as the characteristic equation (25) for perturbation growth rate, where the system stability is shown to depend on the rescaled parameters  $\epsilon^*$ ,  $\eta^*$ , and  $\gamma^*$ , which in fact are all proportional to  $|r|^{-1/2}$  with  $r$  linearly dependent on temperature  $T$  (see Eqs. (24) and (23)). This temperature dependence of stability property can also be obtained from Eq. (26) that has dimension-full form.

It is interesting to compare our theoretical results for instability with the observations of isothermal annealing experiments on strained films. Experiments on SiGe/Si postdeposition system<sup>8,30,31</sup> have exhibited a morphological evolution procedure from an initial planar film surface to a rough surface profile with ripples or islands during annealing. Also, along with this morphological modulation, the Ge segregation has been found on the surface of SiGe layers by Walther *et al.*,<sup>8</sup> which corresponds to the coupling of compositional and morphological instabilities studied here. The temperature effect on the stability of Si<sub>0.5</sub>Ge<sub>0.5</sub> strained films has been investigated by Chen *et al.*<sup>30</sup> They observed that the evolution to unstable surface morphology only occurs above an annealing temperature, and attributed this sharp temperature dependence to the existence of an energy barrier. Our theoretical results (for the case of  $T > T_c^{\text{eff}}$ , *e.g.*, stability diagram like Fig. 3), obtained from the surface diffusion mechanism, can explain this temperature dependent phenomenon without the introduction of an energy barrier. For small temperature  $T$  (but still above  $T_c^{\text{eff}}$ , as in real experiments), we have small  $|r|$  (see Eq. (23)) and then large  $\gamma^*$  (resulting in the large stable region of the stability diagram) and large  $\eta^*$ , which are apt to suppress the instability. When  $T$  increases,

the value of  $\epsilon^*$  becomes smaller, and more importantly,  $\gamma^*$  and  $\eta^*$  also decrease, rendering the system closer to the unstable region of the stability diagram. Thus, one can reach a transition temperature above which the annealing system is unstable, as found in the experiments.

In summary, we have developed a continuum model to study the nonequilibrium evolution processes of strained alloy films in the absence of growth. With the consideration of coupling between surface and bulk states as well as the composition dependence of elastic moduli (both  $E$  and  $\mu$ ), new and more complicated stability results and diagrams have been obtained using linear stability analysis. In general case, joint stability or instability is found due to the coupling between morphological and compositional perturbations. More importantly, the interplay of morphological and compositional strains as well as the composition-dependent elastic constants leads to the stability dependence on the sign of film-substrate misfit, and the possibility of stabilization even for films below  $T_c^{\text{eff}}$ . Here we only study the early film evolution, and the nonlinear effects should be considered for later regimes and for the determination of detailed surface morphologies and patterns.

### Acknowledgments

This work was supported by the NSERC of Canada.

- 
- \* Electronic address: [zfh@physics.utoronto.ca](mailto:zfh@physics.utoronto.ca)  
† Electronic address: [desai@physics.utoronto.ca](mailto:desai@physics.utoronto.ca); URL: <http://www.physics.utoronto.ca/people/faculty/desai.html>
- <sup>1</sup> R. J. Asaro and W. A. Tiller, *Metall. Trans.* **3**, 1789 (1972).
  - <sup>2</sup> M. A. Grinfeld, *Sov. Phys. Dokl.* **31**, 831 (1987).
  - <sup>3</sup> D. J. Srolovitz, *Acta Metall.* **37**, 621 (1989).
  - <sup>4</sup> B. J. Spencer, P. W. Voorhees, and S. H. Davis, *Phys. Rev. Lett.* **67**, 3696 (1991); *J. Appl. Phys.* **73**, 4955 (1993).
  - <sup>5</sup> F. K. LeGoues, M. Copel, and R. M. Tromp, *Phys. Rev. B* **42**, 11690 (1990).
  - <sup>6</sup> D. J. Eaglesham and M. Cerullo, *Phys. Rev. Lett.* **64**, 1943 (1990).
  - <sup>7</sup> Y. H. Xie, G. H. Gilmer, C. Roland, P. J. Silverman, S. K. Buratto, J. Y. Cheng, E. A. Fitzgerald, A. R. Kortan, S. Schuppler, M. A. Marcus, and P. H. Citrin, *Phys. Rev. Lett.* **73**, 3006 (1994).
  - <sup>8</sup> T. Walther, C. J. Humphreys, and A. G. Cullis, *Appl. Phys. Lett.* **71**, 809 (1997).
  - <sup>9</sup> D. D. Perović, B. Bahierathan, H. Lafontaine, D. C. Houghton, and D. W. McComb, *Physica A* **239**, 11 (1997).
  - <sup>10</sup> P. Sutter and M. G. Lagally, *Phys. Rev. Lett.* **84**, 4637 (2000).
  - <sup>11</sup> R. M. Tromp, F. M. Ross, and M. C. Reuter, *Phys. Rev. Lett.* **84**, 4641 (2000).
  - <sup>12</sup> C. W. Snyder, B. G. Orr, D. Kessler, and L. M. Sander, *Phys. Rev. Lett.* **66**, 3032 (1991).
  - <sup>13</sup> M. Gendry, G. Grenet, Y. Robach, P. Krapf, L. Porte, and G. Hollinger, *Phys. Rev. B* **56**, 9271 (1995).
  - <sup>14</sup> J. E. Guyer, S. A. Barnett, and P. W. Voorhees, *J. Crystal Growth* **217**, 1 (2000).
  - <sup>15</sup> T. Okada, G. C. Weatherly, and D. W. McComb, *J. Appl. Phys.* **81**, 2185 (1997).
  - <sup>16</sup> F. Peiró, A. Cornet, J. R. Morante, A. Georgakilas, C. Wood, and A. Christou, *Appl. Phys. Lett.* **66**, 2391 (1995).
  - <sup>17</sup> D. González, G. Aragón, D. Araújo, and R. Garcia, *Appl. Phys. Lett.* **76**, 3236 (2000).
  - <sup>18</sup> J. W. Cahn, *Acta Metall.* **9**, 795 (1961); *Trans. Metall. Soc. AIME* **242**, 166 (1968).
  - <sup>19</sup> F. C. Larché and J. W. Cahn, *Acta Metall.* **33**, 331 (1985).
  - <sup>20</sup> J. E. Guyer and P. W. Voorhees, *Phys. Rev. B* **54**, 11710 (1996); *Mat. Res. Soc. Symp. Proc.* **399**, 351 (1996); *J. Cryst. Growth* **187**, 150 (1998).
  - <sup>21</sup> B. J. Spencer, P. W. Voorhees, and J. Tersoff, *Phys. Rev. Lett.* **84**, 2449 (2000).
  - <sup>22</sup> B. J. Spencer, P. W. Voorhees, and J. Tersoff, *Appl. Phys. Lett.* **76**, 3022 (2000); *Phys. Rev. B* **64**, 235318 (2001).
  - <sup>23</sup> P. Venezuela and J. Tersoff, *Phys. Rev. B* **58**, 10871 (1998).
  - <sup>24</sup> F. Léonard and R. C. Desai, *Phys. Rev. B* **57**, 4805 (1998).
  - <sup>25</sup> F. Léonard and R. C. Desai, *Appl. Phys. Lett.* **74**, 40 (1999).
  - <sup>26</sup> Z. F. Huang and R. C. Desai, submitted to *Phys. Rev. B*.
  - <sup>27</sup> F. Glas, *Phys. Rev. B* **55**, 11277 (1997).
  - <sup>28</sup> P. Kumar and K. Maki, *Phys. Rev. B* **13**, 2011 (1976).
  - <sup>29</sup> W. W. Mullins, *J. Appl. Phys.* **28**, 333 (1957).
  - <sup>30</sup> K. M. Chen, D. E. Jesson, S. J. Pennycook, T. Thundat, and R. J. Warmack, *J. Vac. Sci. Technol. B* **14**, 2199 (1996).
  - <sup>31</sup> C. S. Ozkan, W. D. Nix, and H. Gao, *Mat. Res. Soc. Symp. Proc.* **440**, 323 (1997).
  - <sup>32</sup> B. J. Spencer, P. W. Voorhees, S. H. Davis, and G. B. McFadden, *Acta Metall. Mater.* **40**, 1599 (1992).

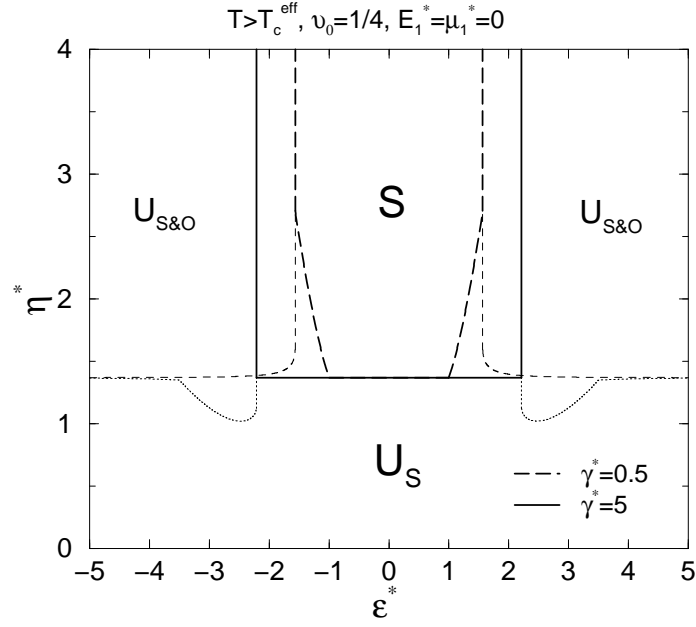


FIG. 1: Stability diagram for non-growing strained alloy film with  $E_1^* = \mu_1^* = 0$ , temperature  $T > T_c^{\text{eff}}$ , and  $\nu_0 = 1/4$ . Region marked by “S” is the stable region. Long dashed and solid thick lines denote the stability boundaries for  $\gamma^* = 0.5$  and 5, respectively. In the unstable region, the domain marked as “U<sub>S</sub>” corresponds to steady instability and that marked as “U<sub>S&O</sub>” corresponds to steady or oscillatory instabilities depending on the wavenumber  $k$ . The boundaries between “U<sub>S</sub>” and “U<sub>S&O</sub>” regions are indicated by dashed ( $\gamma^* = 0.5$ ) and dotted ( $\gamma^* = 5$ ) thin curves.

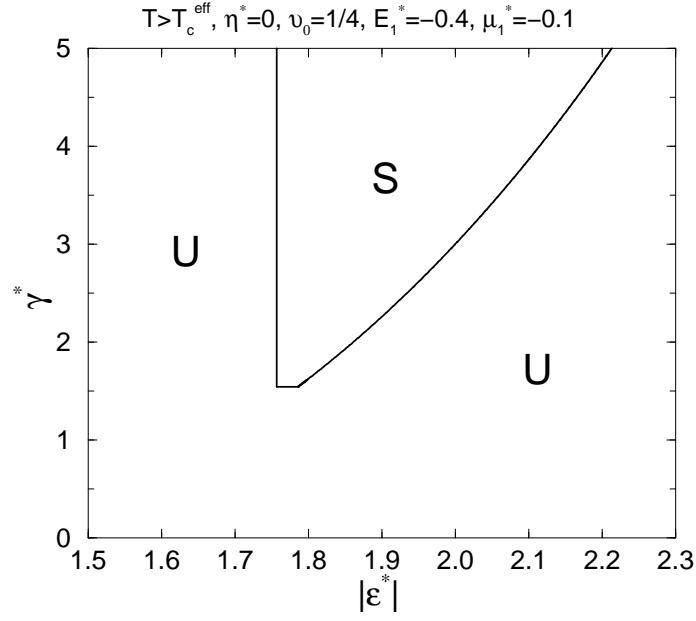


FIG. 2: Stability diagram for  $\eta^* = 0$  non-growing strained alloy film, with  $T > T_c^{\text{eff}}$ ,  $\nu_0 = 1/4$ ,  $E_1^* = -0.4$ , and  $\mu_1^* = -0.1$ . Stable and unstable regions are marked as “S” and “U”, respectively.

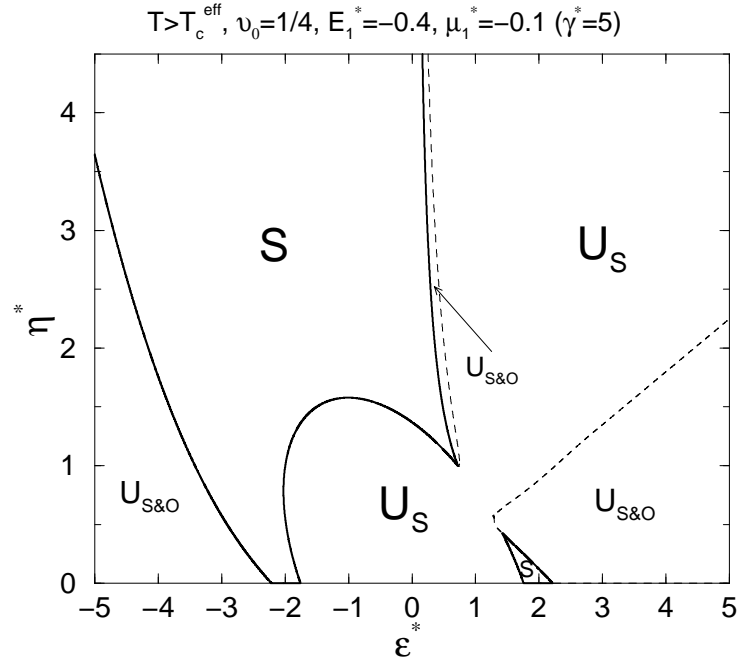


FIG. 3: Stability diagram for non-growing strained alloy film with  $T > T_c^{\text{eff}}$ . Parameters of Set 1 are chosen:  $E_1^* = -0.4$ ,  $\mu_1^* = -0.1$ ,  $\nu_0 = 1/4$ , and  $\gamma^* = 5$ . Stable and unstable regions are marked in a manner similar to that in Fig. 1.

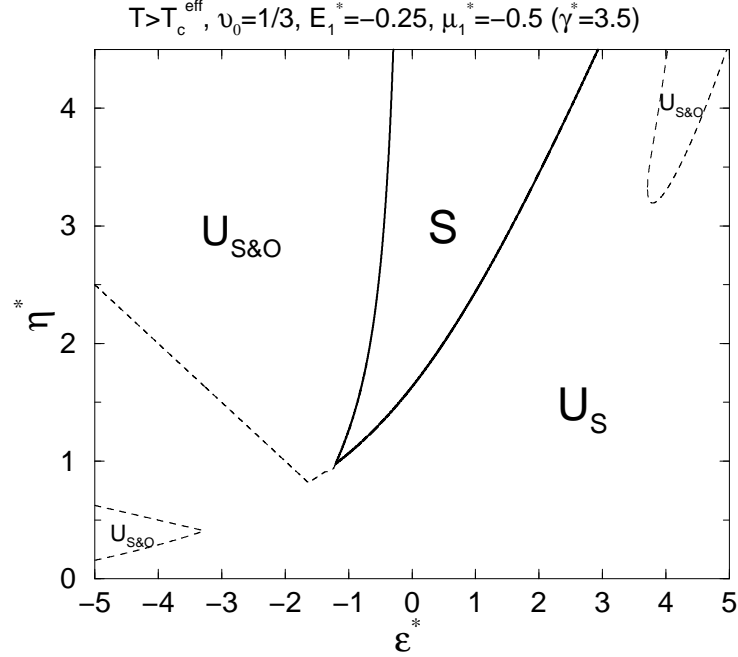


FIG. 4: Stability diagram for  $T > T_c^{\text{eff}}$  strained alloy film in the absence of growth, with Set 2 parameters:  $E_1^* = -0.25$ ,  $\mu_1^* = -0.5$ ,  $\nu_0 = 1/3$ , and  $\gamma^* = 3.5$ . Regions with different stability properties are marked as in Figs. 1 and 3.

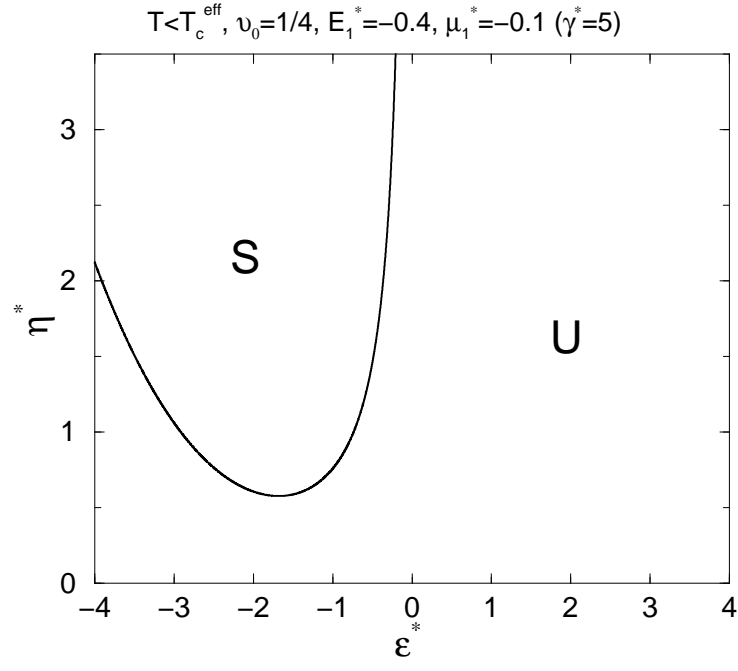


FIG. 5: Stability diagram for non-growing strained alloy film with  $T < T_c^{\text{eff}}$  and composition-dependent elastic moduli. The parameters are of Set 1 as described in Fig. 3.

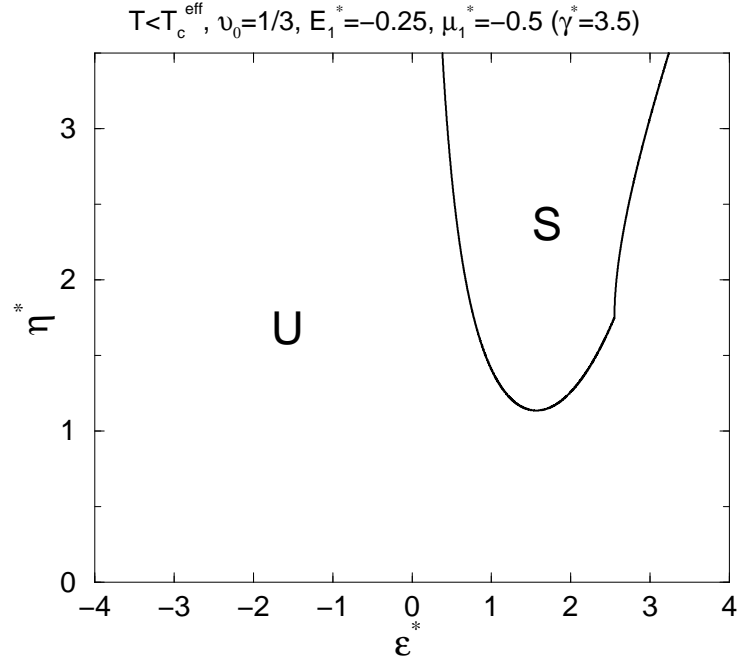


FIG. 6: Stability diagram for non-growing strained alloy film with  $T < T_c^{\text{eff}}$  as well as the Set 2 parameters as described in Fig. 4.